

Deep Unfolding of Iteratively Reweighted ADMM for Wireless RF Sensing

Udaya S.K.P. Miriya Thanthrige, Peter Jung, and Aydin Sezgin

Abstract—We address the detection of material defects, which are inside a layered material structure using compressive sensing based multiple-input and multiple-output (MIMO) wireless radar. Here, the strong clutter due to the reflection of the layered structure’s surface often makes the detection of the defects challenging. Thus, sophisticated signal separation methods are required for improved defect detection. In many scenarios, the number of defects that we are interested in is limited and the signaling response of the layered structure can be modeled as a low-rank structure. Therefore, we propose joint rank and sparsity minimization for defect detection. In particular, we propose a non-convex approach based on the iteratively reweighted nuclear and ℓ_1 -norm (a double-reweighted approach) to obtain a higher accuracy compared to the conventional nuclear norm and ℓ_1 -norm minimization. To this end, an iterative algorithm is designed to estimate the low-rank and sparse contributions. Further, we propose deep learning to learn the parameters of the algorithm (i.e., algorithm unfolding) to improve the accuracy and the speed of convergence of the algorithm. Our numerical results show that the proposed approach outperforms the conventional approaches in terms of mean square errors of the recovered low-rank and sparse components and the speed of convergence.

I. INTRODUCTION

Non-destructive testing (NDT) is important in many areas such as remote sensing, security, and many more [1], [2]. Further, NDT plays an important role in many industrial applications because it does not cause damage to the material under test. The electromagnetic (EM) waves-based remote sensing has many potential industrial applications such as identification of inflammable materials [3], behind the wall object identification [4], multi-layer target detection [5], material characterization [6], and defect detection [7]. In EM waves-based detection of objects/defects which are behind or inside a layered structure, i.e., sub-layer objects/defects identification, the EM waves that reflect from the object/defect are analyzed. Here, one major challenge is the presence of

strong unwanted reflections, i.e., clutter [8], [9]. In the EM waves-based object/defect detection, the main source of the clutter is the reflection from the surface of the layered material structure. In addition to that, multiple reflections between the antenna and the surface of the layered structure also act as a clutter.

The simplest clutter reduction approach is the background subtraction (BS). In addition to that the spatial filtering (SF) [4], and the subspace projection (SP) [10] are widely known clutter suppression methods. The state-of-the-art clutter suppression methods such as BS, SF and SP are not able to suppress the clutter in the context of object/defect detection. This is due to the fact in the BS requires the reference data of the scene and this reference data is not available most of the time. Further, the BS is likely to fail in the time-varying environments in which the background rapidly changing over time. Moreover, in the SP prior knowledge is required to determine the perfect threshold for clutter removal. In addition to that, in SP and SF, a full measurement data set is required. In some cases, it is not possible to acquire full measurement data set due to wireless interference, jamming and sensor failure. Further, clutter suppression becomes even more challenging if objects and clutter are closely located. This occurs regularly in the detection of objects/defects which are inside a layered structure. Then, due to the small delay spread between the signaling responses of objects/defects and clutter superimpose each other. In order to overcome these challenges, advanced signal processing methods are required for clutter suppression. Note that, in many scenarios the number of objects/defects is limited. Therefore, the signaling response of the defect is sparse in nature. By exploring this, compressive sensing (CS) [11] based approaches have shown promising results in object/defect detection [12]–[17]. Also, the CS-based approaches do not require full measurement data set, which results in fast data acquisition and less sensitivity to sensor failure, wireless interference and jamming. Initially, the CS-based approaches assumed that clutter is already removed. However, later joint object detection and clutter removal have been introduced. Here, it is considered that the clutter resides in a low-rank subspace and the response of the objects is sparse [13]–[15], [18], [19]. There are many applications where the data generated by the application can be modeled as a combination of low-rank plus sparse contributions. For instance, in fabric defect detection, the defect-free image results in a low-rank contribution and defective regions result in a sparse contribution [20], [21].

The work of U. S. K. P. M. Thanthrige and A. Sezgin is funded by the Deutsche Forschungsge-meinschaft (DFG, German Research Foundation) Project-ID287022738 TRR 196 (S02) and the work of P. Jung is funded by the German Federal Ministry of Education and Research (BMBF) in the framework of the international future AI lab “AI4EO—Artificial Intelligence for Earth Observation: Reasoning, Uncertainties, Ethics and Beyond” (Grant number: 01DD20001).

U. S. K. P. M. Thanthrige and A. Sezgin are with the Institute of Digital Communication Systems (DCS), Ruhr University Bochum (RUB), 44801 Bochum, Germany. Email: {udaya.miriyathanthrige, aydin.sezgin}@rub.de.

P. Jung is with the Institute of Communications and Information Theory, Technical University Berlin, 10587 Berlin, Germany and Data Science in Earth Observation, Technical University of Munich, 82024 Taufkirchen/Ottobrunn, Germany. Email: peter.jung@tu-berlin.de.

“This work has been submitted for possible publication. Copyright may be transferred without notice, after which this version may no longer be accessible.”

To this end, for the general data acquisition model the received data vector $\mathbf{y} \in \mathbb{C}^K$ is modelled as a combination of low-rank matrix $\mathbf{L} \in \mathbb{C}^{M \times N}$ and a sparse matrix $\mathbf{S} \in \mathbb{C}^{M \times N}$

$$\mathbf{y} = \mathbf{A}_l \text{vec}(\mathbf{L}) + \mathbf{A}_s \text{vec}(\mathbf{S}) + \mathbf{n}. \quad (1)$$

Here, $\mathbf{A}_l, \mathbf{A}_s \in \mathbb{C}^{K \times MN}$ with $K \ll MN$, $\mathbf{n} \in \mathbb{C}^{K \times 1}$ are compression operators and measurement noise, respectively. Further, $\text{vec}(\cdot)$ denotes the vectorization operator, which converts a matrix to a vector by stacking the columns of the matrix. Given the received data vector \mathbf{y} our aim to estimate the signals of interest (\mathbf{L} and \mathbf{S}) using a few number of linear measurement. Note that estimating a low-rank matrix and a sparse vector or matrix from the observations is widely known as robust principal component analysis (RPCA) [22], [23].

Estimating a matrix with the lowest rank and the sparsest matrix from the compressed observations are usually NP-hard problems and thus difficult to solve. To this end, convex relaxations of sparsity (ℓ_0 -norm: the number of nonzero components) and rank in terms of ℓ_1 -norm of a matrix (absolute sum of elements) and nuclear norm of a matrix (sum of singular values of a matrix) are utilized, respectively [24]–[30].

The major difference between the ℓ_1 -norm minimization and the ℓ_0 -norm minimization is that the ℓ_1 -norm minimization depends on the magnitudes of the elements of a signal. Due to this key difference, in the ℓ_1 -norm minimization, larger coefficients are heavily penalized while smaller coefficients are less penalized compared to the ℓ_0 -norm minimization [31]. Further, the ℓ_1 -norm minimization is a loose approximation of the ℓ_0 -norm minimization. Thus, the solution of the ℓ_1 -norm minimization is sub-optimal to the solution of the ℓ_0 -norm minimization. Note that in many applications, the important properties/features are preserved by the large coefficients of the signal. Similarly, the large singular values of the received signal matrix capture the important features of the data. However, the nuclear norm minimization algorithms shrink all the singular values with the same threshold. Thus, to avoid this weakness we should shrink more the smaller singular values while shrink less the larger singular value. Therefore, in both ℓ_1 -norm minimization and nuclear norm minimization, the reweighted ℓ_1 -norm minimization and reweighted nuclear norm minimization have been considered to minimize the imbalance in both ℓ_1 -norm minimization and nuclear norm minimization.

Note that, non-convex approaches, i.e., reweighted nuclear norm and ℓ_1 -norm minimization have shown better performance over the convex relaxations by providing tighter characterizations of rank and sparsity. For instance studies [31], [32] have shown that the reweighted ℓ_1 -norm minimization outperforms the ℓ_1 -norm minimization. Similarly, studies [33], [34] have shown that the reweighted nuclear norm outperforms the nuclear norm minimization.

To this end, we formulate an optimization problem based on the reweighted nuclear norm and ℓ_1 -norm minimization to jointly estimate the low-rank matrix and the sparse vector from

few compressive measurements. Then, the estimated sparse vector is used to identify defects. In particular, we propose a novel approach by considering the full doubly-reweighted approach, i.e., wrt. nuclear and ℓ_1 - norm. To the best of our knowledge, this has not yet been studied in the literature for the compressive case. Next, we consider an iterative algorithm based on the alternating direction method of multipliers (ADMM) [35] to jointly estimate the low-rank matrix and the sparse vector from few compressive measurements.

In this work, to solve the reweighted ℓ_1 -norm minimization and the reweighted nuclear norm minimization problems, we propose the element-wise soft thresholding and the element-wise singular value thresholding (the element-wise soft thresholding of singular values of the matrix). Note that, the element-wise soft thresholding applies different thresholds for each element. Since the element-wise soft thresholding/element-wise singular value thresholding treats each element of the matrix/singular value differently, it provides flexibility to shrink more the smaller values while shrink less large values. In this context, the selection of suitable values for the soft thresholding and the singular value thresholding are important. Generally, thresholds are chosen by handcrafting, and it is a time consuming task. Further, the accuracies of the recovered low-rank and sparse components are heavily dependent on the proper selection of the threshold parameters. As an example in soft thresholding, if the threshold is too high then it makes many coefficients to be zero and if the threshold is too low then there are many non-zero coefficients. Further, the selection of proper thresholds in the iterative algorithms improves their convergence rates. Therefore, the wrong selection of thresholding parameters reduces the convergence rate of the iterative algorithm. Hence, it requires a large number of iterations to converge to the desired solution. Therefore, in this work, we propose deep learning-based parameter learning to improve the accuracies of the recovered low-rank and sparse components and the convergence rate of the ADMM based iterative algorithm.

The deep learning based algorithm unrolling/unfolding is an emerging research field that has shown promising results in many applications such as sparse vector recovery (sparse coding) [36]–[38], image processing [39]–[41] and low-rank plus sparse recovery [42], [43]. Interesting overview of the algorithm unrolling/unfolding can be found in [44], [45]. For example, in [36] they studied the unfolding of the popular iterative shrinkage and thresholding algorithm (ISTA) and coordinate descent (CoD) for sparse vector recovery. They have shown that the learned ISTA (LISTA) converges twenty times faster than the untrained ISTA. Further, in [37] algorithm unfolding with the element-wise adaptive threshold is proposed for ISTA. In-contrast to ISTA, the element-wise adaptive thresholding with ISTA applies different thresholds for each element. These thresholds depend on the previous estimate of the sparse vector. They have shown that the adaptive thresholding scheme has a better convergence rate than the conventional non-adaptive thresholding scheme. Low-rank plus sparse recovery algorithm unfolding for ultrasound imaging was proposed in [42], [43] and it was shown that the unrolled network provides improved convergence speed and

accuracy compared to the untrained iterative algorithm.

A. Contribution

The contributions of this work are summarized as follows:

- We propose the non-convex fully double-reweighted approach i.e., both reweighted ℓ_1 -norm and nuclear norm simultaneously to solve the RPCA problem in the compressive sensing data acquisition model which reflects more the practical problem at hand.
- We propose an iterative algorithm based on ADMM to estimate the low-rank and sparse components jointly.
- We propose a deep neural network (DNN) to learn the parameters of the iterative algorithm (i.e., algorithm unfolding) from the training data.
- We consider two types of data to evaluate our approach. As a practical application, the defect detection by SFCW radar from compressive measurements is used. In addition to that, for a standard benchmark, a generic Gaussian data acquisition model is used. Further, we compare the performance of the proposed DNN based approach with the standard convex approach (i.e., nuclear norm and ℓ_1 -norm minimization) and the untrained ADMM based iterative algorithm. In both cases, our numerical results show that the proposed approach outperforms the conventional approaches in terms of mean squared errors of the recovered low-rank and sparse components and the speed of convergence.

In the following, we emphasize the differences of our approach with the existing approaches in the literature. Most of the work in the literature focus on the standard RPCA which considers both \mathbf{A}_l and \mathbf{A}_s in (1) to be identity matrices [34], [46], [47]. Further, we would like to point out that most of the time RPCA problems are solved by using the convex relaxation, i.e., nuclear norm and ℓ_1 -norm minimization or with the single reweighting, i.e., either reweighted ℓ_1 -norm or reweighted nuclear norm [34], [42], [43], [46]. In this work we study the joint reweighted nuclear norm and reweighted ℓ_1 -norm (full doubly-reweighted) compressive sensing data acquisition model which reflects more the practical problem at hand. In the context of the algorithm unfolding for the low-rank plus sparse recovery problem, [42], [43] are the closest work to our work. However, there are two main differences that we would like to highlight. (a) Both [42], [43] have considered the standard convex relaxation (ℓ_1 -norm and nuclear norm) to solve the RPCA problem, while we propose the reweighted ℓ_1 -norm and reweighted nuclear norm. (b) Different from [42], [43] our focus is on defect detection based on MIMO wireless sensing while [42], [43] focus on ultrasound imaging application.

The remainder of the paper is organized as follows. We introduce the general data acquisition and low-rank plus sparse recovery with reweighting in Section II. In Section III we discuss the DNN-based low-rank plus recovery algorithm unfolding. In Section IV, we provide an evaluation of the proposed DNN-based low-rank plus recovery algorithm unfolding approaches and provide interesting insights. Section V concludes the paper.

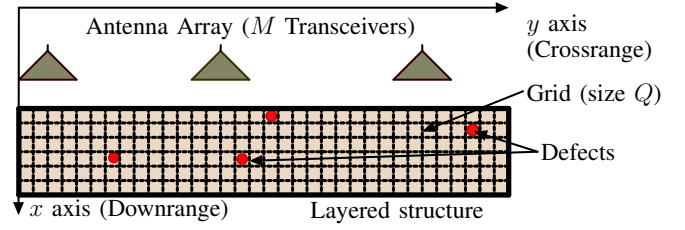


Fig. 1. Getting the measurements of a single-layered material structure using a SFCW radar with M transceivers.

II. SYSTEM MODEL

First, we briefly present the system model of the mono-static stepped-frequency continuous (SFCW) radar-based defect detection. Next, we are going to discuss the general data acquisition model and the alternating direction method of multipliers (ADMM) [35] based iterative algorithm for the low-rank plus sparse recovery.

A. SFCW radar based defect detection by low-rank plus sparse recovery

This section briefly presents the defect detection based on a mono-static stepped-frequency continuous (SFCW) radar. Here, we consider a SFCW radar with M transceivers which are placed in parallel to the single-layered material structure while maintaining an equal distance between transceivers as shown in Fig. 1. In SFCW radar, each transceiver transmits a stepped-frequency signal containing N frequencies which are equally spaced over the bandwidth of B Hz. To this end, the received signal of the m -th transceiver corresponding to n -th frequency band (f_n), $y_{m,n}$ is given by

$$y_{m,n} = y_{m,n}^l + y_{m,n}^d + z_{m,n}. \quad (2)$$

Here, $z_{m,n}$ is the additive Gaussian noise. Note that, $y_{m,n}$ consists of two main components, the reflection of the layered material structure ($y_{m,n}^l$) and the reflection of the defects ($y_{m,n}^d$). Now, the received signal corresponding to all M transceivers and N frequencies $\mathbf{Y} \in \mathbb{C}^{M \times N}$ are given by

$$\mathbf{Y} = \mathbf{Y}^l + \mathbf{Y}^d + \mathbf{Z}. \quad (3)$$

Here, \mathbf{Y}^l , \mathbf{Y}^d and $\mathbf{Z} \in \mathbb{C}^{M \times N}$ are the received signals of the layered structure, defects and noise, respectively. Next, we discuss in details the modeling of the received signal of the defects by using the propagation time delay. To this end, the scene shown in Fig. 1 is hypothetically partitioned into a rectangular grid of size Q . Suppose that the round-travel time of the signal from the m -th antenna location to the p -th defect and back is given by $\tau_{m,p}$. Then, $y_{m,n}^d$ in (2) is given by

$$y_{m,n}^d = \sum_{p=1}^P \alpha_p e^{-j2\pi f_n \tau_{m,p}}. \quad (4)$$

Here, $j = \sqrt{-1}$, $\alpha_p \in \mathbb{C}$ is the complex signal strength of the p -th defect and P is the total number of defects. To this end, $\text{vec}(\mathbf{Y}^d) \in \mathbb{C}^{MN \times 1}$ is given by

$$\text{vec}(\mathbf{Y}^d) = \mathbf{D}\mathbf{s}, \quad (5)$$

where vector $\mathbf{s} \in \mathbb{C}^{Q \times 1}$ contains all the α_p values of the defects. Note that, since there are P defects, the vector \mathbf{s} only contains P non-zero entries. The matrix \mathbf{D} is given by $[(\mathbf{D}_1)^T, \dots, (\mathbf{D}_m)^T, \dots, (\mathbf{D}_M)^T]^T \in \mathbb{C}^{MN \times Q}$. Note that, the (n, q) -th element of the matrix $\mathbf{D}_m \in \mathbb{C}^{N \times Q}$ is given by $\exp(-j2\pi f_n \tau_{m,q})$, where $\tau_{m,q}$ is the propagation time delay between the m -th antenna to the q -th grid location. Note that, we assume that the propagation time delays of the defects are exactly matched with the propagation time delays of the grid locations.

B. Compressed sensing (CS) approach

In this subsection, we are going to discuss the SFCW measurement model with compressed sensing (CS). In the CS setup, we assume that only a subset of antennas and frequencies are available or selected. Now, the reduced data vector $\mathbf{y}_{cs} \in \mathbb{C}^{K \times 1}$ of size $K \ll MN$ is given by

$$\begin{aligned} \mathbf{y}_{cs} &= \Phi(\text{vec}(\mathbf{Y})), \\ &= \Phi \text{vec}(\mathbf{Y}^l) + \Phi \mathbf{D} \mathbf{s} + \Phi \text{vec}(\mathbf{Z}), \end{aligned} \quad (6)$$

where $\Phi \in \mathbb{R}^{K \times MN}$ is the selection matrix. It is used to select a particular antenna and a frequency band. In more details, Φ has a single non-zero element of value 1 in each row to indicate the selected frequency of a particular antenna if that antenna is selected. Here, our main objective is to recover \mathbf{Y}^l and \mathbf{s} from the reduced data vector \mathbf{y}_{cs} using the low-rank plus sparse recovery approach as detailed below.

Next we present the generic measurement model by slightly modifying the data acquisition model given in (6). In particular the SFCW measurement model is mapped to the generic measurement model by consider $\mathbf{A}_s = \Phi \mathbf{D}$, $\mathbf{A}_l = \Phi$, $\mathbf{Y}^l = \mathbf{L}$, $\mathbf{s} = \text{vec}(\mathbf{S})$ and $\mathbf{y}_{cs} = \mathbf{y}$. Now, the measured data vector $\mathbf{y} \in \mathbb{C}^{K \times 1}$ is expressed as a combination of a low-rank matrix $\mathbf{L} \in \mathbb{C}^{M \times N}$ and a sparse matrix $\mathbf{S} \in \mathbb{C}^{M \times N}$ with $M \leq N$ as follows

$$\mathbf{y} = \mathbf{A}_l \text{vec}(\mathbf{L}) + \mathbf{A}_s \text{vec}(\mathbf{S}) + \mathbf{n}. \quad (7)$$

Here, $\mathbf{A}_l, \mathbf{A}_s \in \mathbb{C}^{K \times MN}$, $\mathbf{n} \in \mathbb{C}^{K \times 1}$ are compression operators and measurement noise, respectively. Our objective is to recover the low-rank matrix \mathbf{L} and the sparse matrix \mathbf{S} from the compressive measurements \mathbf{y} given in (7). Thus, the estimation of \mathbf{L} and \mathbf{S} from \mathbf{y} is formulated as a low-rank plus sparse recovery problem as

$$\begin{aligned} \{\hat{\mathbf{L}}, \hat{\mathbf{S}}\} &= \arg \min_{\mathbf{L}, \mathbf{S}} \lambda_l \text{rank}(\mathbf{L}) + \lambda_s \|\mathbf{S}\|_0, \\ \text{s.t. } &\|\mathbf{y} - \mathbf{A}_s \text{vec}(\mathbf{S}) - \mathbf{A}_l \text{vec}(\mathbf{L})\|_2^2 \leq \epsilon. \end{aligned} \quad (8)$$

Here, λ_l, λ_s are regularization parameters and ϵ is a small positive constant (noise bound). Here, $\|\cdot\|_0$ is the ℓ_0 -norm of the matrix and $\text{rank}(\cdot)$ is the rank of the matrix. Note that, rank and ℓ_0 -norm minimization problems are usually NP-hard. Thus, one may use convex relaxations based on the nuclear norm of a matrix and ℓ_1 -norm of a matrix. To this end, the estimation of \mathbf{L} and \mathbf{S} from \mathbf{y} is formulated as

$$\begin{aligned} \{\hat{\mathbf{L}}, \hat{\mathbf{S}}\} &= \arg \min_{\mathbf{L}, \mathbf{S}} \lambda_l \|\mathbf{L}\|_* + \lambda_s \|\mathbf{S}\|_1, \\ \text{s.t. } &\|\mathbf{y} - \mathbf{A}_s \text{vec}(\mathbf{S}) - \mathbf{A}_l \text{vec}(\mathbf{L})\|_2^2 \leq \epsilon. \end{aligned} \quad (9)$$

Here, $\|\cdot\|_1, \|\cdot\|_*$ are the ℓ_1 -norm and nuclear norm of a matrix, respectively. The resulting convex problems, i.e., ℓ_1 -norm and nuclear norm minimization are well studied in the literature and there are several non-convex approaches to improve over the standard convex relaxation. One well-known approach is iterative reweighting of the ℓ_1 -norm [31], [48] and nuclear norm [34], [49]–[51]. In this work, we consider a double-reweighted approach, i.e., both reweighted ℓ_1 -norm and nuclear norm simultaneously. The problem given in (9) is challenging due to its convex multi-objective nature. Thus, the alternating direction method of multipliers (ADMM) is used to solve this problem [35]. First, we formulate the problem given in (9) based on the ADMM approach, and then we introduce the non-convex double-reweighted approach.

Now, we define a Lagrangian function (called augmented Lagrangian function) for the problem given in (9) as follows.

$$\begin{aligned} L(\mathbf{L}, \mathbf{S}, \mathbf{u}) &= \lambda_l \|\mathbf{L}\|_* + \lambda_s \|\mathbf{S}\|_1 + \\ &\langle \mathbf{u}, \mathbf{A}_s \text{vec}(\mathbf{S}) + \mathbf{A}_l \text{vec}(\mathbf{L}) - \mathbf{y} \rangle + \\ &\frac{\rho}{2} \|\mathbf{A}_s \text{vec}(\mathbf{S}) + \mathbf{A}_l \text{vec}(\mathbf{L}) - \mathbf{y}\|_2^2. \end{aligned} \quad (10)$$

Here, $\mathbf{u}, \rho > 0$ are auxiliary variables and a penalty factor, respectively. The $\langle \cdot \rangle$ denotes the standard trace inner product. The optimization problem in (10) is solved by alternatively optimizing each component. Let the signal component value of \mathbf{S}, \mathbf{L} and \mathbf{u} at the t -th iteration be denoted as $(\cdot)^t$. For instance, the signal component value of \mathbf{L} at the $(t+1)$ -th iteration is given by $(\mathbf{L})^{t+1}$. To update \mathbf{L} at the $(t+1)$ -th iteration, the following optimization problem is solved while keeping $(\mathbf{S})^t$ and $(\mathbf{u})^t$ fixed.

$$\begin{aligned} (\mathbf{L})^{t+1} &= \arg \min_{\mathbf{L}} \lambda_l \|\mathbf{L}\|_* + \frac{\rho}{2} \|\mathbf{A}_s \text{vec}((\mathbf{S})^t) \\ &+ \mathbf{A}_l \text{vec}(\mathbf{L}) - \mathbf{y} + \frac{1}{\rho} (\mathbf{u})^t\|_2^2, \\ &= \arg \min_{\mathbf{L}} \lambda_l \|\mathbf{L}\|_* + \frac{\rho}{2} \|\mathbf{A}_l \text{vec}(\mathbf{L}) \\ &- \left(\mathbf{y} - \mathbf{A}_s \text{vec}((\mathbf{S})^t) - \frac{1}{\rho} (\mathbf{u})^t \right)\|_2^2, \\ &= \arg \min_{\mathbf{L}} \lambda_l \|\mathbf{L}\|_* + \frac{\rho}{2} \|\mathbf{A}_l \text{vec}(\mathbf{L}) - \mathbf{y}_l\|_2^2, \end{aligned} \quad (11)$$

where $\mathbf{y}_l = \mathbf{y} - \mathbf{A}_s \text{vec}((\mathbf{S})^t) - \frac{1}{\rho} (\mathbf{u})^t$. Next, \mathbf{S} is updated as (while keeping $(\mathbf{L})^{t+1}$ and $(\mathbf{u})^t$ fixed)

$$\begin{aligned} (\mathbf{S})^{t+1} &= \arg \min_{\mathbf{S}} \lambda_s \|\mathbf{S}\|_1 + \frac{\rho}{2} \|\mathbf{A}_s \text{vec}(\mathbf{S}) \\ &+ \mathbf{A}_l \text{vec}((\mathbf{L})^{t+1}) - \mathbf{y} + \frac{1}{\rho} (\mathbf{u})^t\|_2^2, \\ &= \arg \min_{\mathbf{S}} \lambda_s \|\mathbf{S}\|_1 + \frac{\rho}{2} \|\mathbf{A}_s \text{vec}(\mathbf{S}) \\ &- \left(\mathbf{y} - \mathbf{A}_l \text{vec}((\mathbf{L})^{t+1}) - \frac{1}{\rho} (\mathbf{u})^t \right)\|_2^2, \\ &= \arg \min_{\mathbf{S}} \lambda_s \|\mathbf{S}\|_1 + \frac{\rho}{2} \|\mathbf{A}_s \text{vec}(\mathbf{S}) - \mathbf{y}_s\|_2^2, \end{aligned} \quad (12)$$

where $\mathbf{y}_s = \mathbf{y} - \mathbf{A}_l \text{vec}((\mathbf{L})^{t+1}) - \frac{1}{\rho}(\mathbf{u})^t$. Next, \mathbf{u} is updated by

$$(\mathbf{u})^{t+1} = (\mathbf{u})^t + \rho \left(\mathbf{A}_s \text{vec}((\mathbf{S})^{t+1}) + \mathbf{A}_l \text{vec}((\mathbf{L})^{t+1}) - \mathbf{y} \right). \quad (13)$$

Now, we are going to introduce the weighted ℓ_1 -norm [31], [48] and nuclear norm [34], [49]–[51] to the sub-problems given in (11) and (12). First, we rearrange (11) and (12) as given below.

$$(\mathbf{L})^{t+1} = \arg \min_{\mathbf{L}} \lambda_l \|\mathbf{L}\|_* + f_l(\mathbf{L}). \quad (14)$$

$$(\mathbf{S})^{t+1} = \arg \min_{\mathbf{S}} \lambda_s \|\mathbf{S}\|_1 + f_s(\mathbf{S}), \quad (15)$$

Note that $f_s(\mathbf{S}) = \frac{\rho}{2} \|\mathbf{A}_s \text{vec}(\mathbf{S}) - \mathbf{y}_s\|_2^2$ and $f_l(\mathbf{L}) = \frac{\rho}{2} \|\mathbf{A}_l \text{vec}(\mathbf{L}) - \mathbf{y}_l\|_2^2$ belong to the most widely used squared loss function family and these functions are smooth convex functions [37]. Next, we are going to introduce non-convex concave surrogates for the ℓ_0 -norm and rank as follows.

$$(\mathbf{L})^{t+1} = \arg \min_{\mathbf{L}} \lambda_l \sum_{i=1}^M G_l(\sigma_i(\mathbf{L})) + f_l(\mathbf{L}), \quad (16)$$

$$(\mathbf{S})^{t+1} = \arg \min_{\mathbf{S}} \lambda_s \sum_{m=1, n=1}^{m=M, n=N} G_s(|s_{m,n}|) + f_s(\mathbf{S}), \quad (17)$$

where $s_{m,n}$ is the m -th row and n -th column element of the matrix \mathbf{S} and $\sigma_i(\mathbf{L})$ denotes the i -th singular value of the matrix $\mathbf{L} \in \mathbb{C}^{M \times N}$ and we assume that $M \leq N$. Here, $G_s(\cdot)$ and $G_l(\cdot)$ are concave surrogates for the ℓ_0 -norm and rank, respectively. There are several concave surrogate functions are proposed in the literature and an overview of many known non-convex surrogates for the nuclear norm is given in [52]. These non-convex surrogates are known to perform better compared to the standard convex relaxations (i.e., nuclear norm and ℓ_1 -norm) by providing tighter characterizations of rank and sparsity. These surrogate functions have the following properties [37], [52]. (a) These surrogate functions are concave and monotonically increasing on $[0, \infty)$. (b) Gradients of the surrogate functions are non-negative and monotonically decreasing. Based on these properties and using the majorization-minimization (MM) strategy [53], it can be shown that the non-convex optimization problems given in (16) and (17) can be formulated as iteratively reweighted nuclear norm and ℓ_1 -norm minimization problems as given below [37], [52].

$$\begin{aligned} (\mathbf{L})^{t+1} &= \arg \min_{\mathbf{L}} \lambda_l \sum_{i=1}^M g_l(\sigma_i((\mathbf{L})^t)) \sigma_i(\mathbf{L}) + f_l(\mathbf{L}), \\ &= \arg \min_{\mathbf{L}} \lambda_l \|\mathbf{w}_l^t \odot \boldsymbol{\sigma}(\mathbf{L})\|_1 + f_l(\mathbf{L}), \end{aligned} \quad (18)$$

$$\begin{aligned} (\mathbf{S})^{t+1} &= \arg \min_{\mathbf{S}} \lambda_s \|g_s(|(\mathbf{S})^t|) \odot \mathbf{S}\|_1 + f_s(\mathbf{S}), \\ &= \arg \min_{\mathbf{S}} \lambda_s \|\mathbf{w}_s^t \odot \mathbf{S}\|_1 + f_s(\mathbf{S}). \end{aligned} \quad (19)$$

Here, $g_s(\cdot)$ and $g_l(\cdot)$ are derivatives of $G_s(\cdot)$ and $G_l(\cdot)$, respectively. The operator \odot denotes element-wise multiplication.

Note that, $\boldsymbol{\sigma}(\mathbf{L}) = [\sigma_1, \dots, \sigma_i, \dots, \sigma_M] \in \mathbb{R}^M$ are the singular values of the matrix \mathbf{L} . Here, $\mathbf{w}_l^t \in \mathbb{R}^M$ and $\mathbf{w}_s^t \in \mathbb{R}^{MN}$ are non-negative weight vectors. Here, $w_{l,i}$ is the i -th element of the \mathbf{w}_l^t . To this end, \mathbf{w}_l^t and \mathbf{w}_s^t are given by

$$\mathbf{w}_l^t = g_l(\boldsymbol{\sigma}((\mathbf{L})^t)), \quad (20)$$

$$\mathbf{w}_s^t = g_s(|(\mathbf{S})^t|). \quad (21)$$

Note that the optimization problems are given in (18) and (19) are solved in closed-form by using proximal operators. To be more precise, we consider the element-wise singular value thresholding (i.e., element-wise soft thresholding on the singular value of a matrix) [55] and the element-wise soft thresholding [37] as proximal operators to solve optimization problems are given in (18) and (19), respectively. Now, (18) is solved by

$$(\mathbf{L})^{t+1} = \text{SVT}_{\lambda_{LT}} \left(\mathbf{A}_l^* \left(\mathbf{y} - \mathbf{A}_s \text{vec}((\mathbf{S})^t) + \frac{1}{\rho}(\mathbf{u})^t \right) \right). \quad (22)$$

Similarly, the problem given in (19) is solved by

$$(\mathbf{S})^{t+1} = \text{ST}_{\lambda_{ST}} \left(\mathbf{A}_s^* \left(\mathbf{y} - \mathbf{A}_l \text{vec}((\mathbf{L})^{t+1}) + \frac{1}{\rho}(\mathbf{u})^t \right) \right), \quad (23)$$

where $\text{SVT}(\cdot)$ and $\text{ST}(\cdot)$ are the element-wise singular value and element-wise soft thresholding operators [37], [55], respectively. Note that, $(\cdot)^*$ is a linear operator which back project the vector in to the target matrix subspace. There are two options for $(\cdot)^*$. (a) Hermitian transpose $(\cdot)^H$ as done in [37]. (b) Moore–Penrose pseudo inverse $(\cdot)^\dagger$ as done in [18]. In the next subsection, we are going to discuss the element-wise soft thresholding in more details.

C. Element-wise soft thresholding

Consider (23) and let the intermediate value in the $t+1$ -iteration as $(\mathbf{S}_I)^{t+1} \in \mathbb{C}^{M \times N}$ before the soft thresholding be given by

$$(\mathbf{S}_I)^{t+1} = \mathbf{A}_s^\dagger \left(\mathbf{y} - \mathbf{A}_l \text{vec}((\mathbf{L})^{t+1}) + \frac{1}{\rho}(\mathbf{u})^t \right). \quad (24)$$

To estimate the sparse component in the $t+1$ -th iteration $(\mathbf{S})^{t+1}$, element-wise soft thresholding is applied to each element of the matrix $(\mathbf{S}_I)^{t+1}$ individually. Here, the threshold value is different from element to element. To this end, the element-wise soft thresholding operation of the m -th row and n -th column element of the matrix $(\mathbf{S}_I)^{t+1}$ is defined as

$$\text{ST}_{\lambda_{ST}^{m,n}}(s_{m,n}^{t+1}) = \exp(j\theta) \max(|s_{m,n}^{t+1}| - \lambda_{ST}^{m,n}, 0). \quad (25)$$

Here, θ is the phase angle of the $s_{m,n}^{t+1}$ in radians. Here, $\lambda_{ST}^{m,n}$ is the threshold value related to the element $s_{m,n}^{t+1}$. Note that the threshold value of each element depends on the previous estimate of the element. Also note that the threshold values $(\lambda_{ST}^{m,n} \forall m, n)$ change from iteration to iteration. However, for better readability we not include the index t . To this end, $\lambda_{ST}^{m,n}$ is given by

$$\lambda_{ST}^{m,n} = \lambda_s \times g_s(|s_{m,n}^t|). \quad (26)$$

Here, $g_s(\cdot)$ is a derivative of the non-convex concave surrogate of the ℓ_0 -norm $G_s(\cdot)$ and λ_S is a positive constant. In (26) $s_{m,n}^t$ is the m -th row and n -th column element of the t -th estimation of the sparse component $((\mathbf{S})^t)$. There are several functions proposed in the literature for the concave surrogate and an overview of many known non-convex surrogates for the ℓ_1 -norm and the nuclear norm is given in [52]. In this work, we consider the common log-determinant heuristic [31] and exponential decay [49], [56] as surrogate functions as given below. Here, the log-determinant heuristic is given by

$$G_{\log}(\theta) = \log(\theta + \gamma), \quad (27)$$

while the derivative of $G_{\log}(\theta)$ is given by

$$g_{\log}(\theta) = \frac{1}{\theta + \gamma}. \quad (28)$$

Similarly, the exponential decay heuristic is given by

$$G_{\exp}(\theta) = 1 - \exp\left(\frac{-\theta}{\gamma}\right), \quad (29)$$

while the derivative of $G_{\exp}(\theta)$ is given by

$$g_{\exp}(\theta) = \frac{1}{\gamma} \exp\left(\frac{-\theta}{\gamma}\right). \quad (30)$$

Here, γ is a positive constant. Note that the problems given in (18) and (19) reduce to the standard nuclear norm and ℓ_1 -norm minimization problems when $G_s(\cdot)$ and $G_l(\cdot)$ given in (16) and (17) are equal to $G_s(\theta) = G_l(\theta) = |\theta|$ and $g_s(\theta)$ and $g_l(\theta)$ given in (18) and (19) are equal to $g_s(\theta) = g_l(\theta) = 1$, respectively.

To this end, the estimation of matrix \mathbf{S} in $(t+1)$ -th iteration, i.e., $(\mathbf{S})^{t+1}$ is given by

$$\begin{aligned} (\mathbf{S})^{t+1} &= \text{ST}_{\lambda_{ST}} \left(\mathbf{A}_s^\dagger \left(\mathbf{y} - \mathbf{A}_l \text{vec}((\mathbf{L})^{t+1}) + \frac{1}{\rho}(\mathbf{u})^t \right) \right), \\ &= \text{ST}_{\lambda_{ST}} ((\mathbf{S}_I)^{t+1}), \end{aligned} \quad (31)$$

where $\lambda_{ST} = [\lambda_{ST}^{1,1}, \dots, \lambda_{ST}^{m,n}, \dots, \lambda_{ST}^{M,N}]$ contains different threshold values for each element of \mathbf{S} for the $t+1$ iteration. These threshold values are derived based on the previous estimate of \mathbf{S} , i.e., based on $(\mathbf{S})^t$. To this end, $\lambda_{ST}^{m,n}$ is estimated as follows. Based on the log-determinant heuristic $\lambda_{ST}^{m,n}$ is given by

$$\lambda_{ST}^{m,n} = \lambda_S g_s(s_{m,n}^t) = \lambda_S g_{\log}(s_{m,n}^t) = \frac{\lambda_S}{(\gamma + |s_{m,n}^t|)}, \forall m, n. \quad (32)$$

Based on the exponential decay heuristic $\lambda_{ST}^{m,n}$ is given by

$$\lambda_{ST}^{m,n} = \lambda_S g_s(s_{m,n}^t) = \lambda_S g_{\exp}(s_{m,n}^t) = \frac{\lambda_S}{\gamma} \exp\left(\frac{-|s_{m,n}^t|}{\gamma}\right), \forall m, n. \quad (33)$$

The same concept is also applied to the singular value thresholding which is used to solve the problem given in (22) as discussed next. In this work, we consider the same surrogate function for both ℓ_0 -norm and rank, i.e., $G_s(\cdot) = G_l(\cdot)$. Next, we are going to discuss the element-wise singular value thresholding in more detail.

D. Element-wise singular value thresholding

First, consider (22) and let the intermediate value in $t+1$ -iteration, $(\mathbf{L}_I)^{t+1} \in \mathbb{C}^{M \times N}$ before applying the singular value thresholding be given by

$$(\mathbf{L}_I)^{t+1} = \mathbf{A}_l^\dagger \left(\mathbf{y} - \mathbf{A}_s \text{vec}((\mathbf{S})^t) + \frac{1}{\rho}(\mathbf{u})^t \right). \quad (34)$$

The singular value decomposition of the matrix $(\mathbf{L}_I)^{t+1} \in \mathbb{C}^{M \times N}$ with $M \leq N$ is given as

$$(\mathbf{L}_I)^{t+1} = \mathbf{U} \mathbf{\Lambda} \mathbf{V}^T. \quad (35)$$

Here, $\mathbf{U} \in \mathbb{C}^{M \times M}$ and $\mathbf{V} \in \mathbb{C}^{N \times N}$ are the matrices of left and right singular vectors. $\mathbf{\Lambda} \in \mathbb{R}^{M \times N}$ is a rectangular diagonal matrix with $\boldsymbol{\sigma}(\mathbf{L}) = [\sigma_1, \dots, \sigma_i, \dots, \sigma_M]$ on the diagonal and zeros elsewhere. Next, the element-wise singular value thresholding of the matrix $(\mathbf{L}_I)^{t+1}$ for a given threshold vector $\boldsymbol{\lambda}_{LT} = [\lambda_{LT}^1, \dots, \lambda_{LT}^i, \dots, \lambda_{LT}^M]$ is given by

$$\text{SVT}_{\boldsymbol{\lambda}_{LT}}((\mathbf{L}_I)^{t+1}) = \mathbf{U} \text{diag}(\text{ST}_{\boldsymbol{\lambda}_{LT}}(\boldsymbol{\sigma}(\mathbf{L}_I))) \mathbf{V}^T. \quad (36)$$

Note that, here $\text{ST}_{\boldsymbol{\lambda}_{LT}}(\cdot)$ is the element-wise soft thresholding operator as discussed in II-C and the operator $\text{diag}(\cdot)$ takes a vector as an input and returns a square diagonal matrix in which the main diagonal contains the vector elements and zeros elsewhere. Now, the estimation of the matrix \mathbf{L} in $(t+1)$ -th iteration is given by

$$\begin{aligned} (\mathbf{L})^{t+1} &= \text{SVT}_{\boldsymbol{\lambda}_{LT}} \left(\mathbf{A}_l^\dagger \left(\mathbf{y} - \mathbf{A}_s \text{vec}((\mathbf{S})^t) + \frac{1}{\rho}(\mathbf{u})^t \right) \right), \\ &= \text{SVT}_{\boldsymbol{\lambda}_{LT}} ((\mathbf{L}_I)^{t+1}), \end{aligned} \quad (37)$$

where $\boldsymbol{\lambda}_{LT} = [\lambda_{LT}^1, \dots, \lambda_{LT}^i, \dots, \lambda_{LT}^M]$ contains the different threshold values and λ_{LT}^i is calculated based on the singular values of the previous estimate of matrix \mathbf{L} as given below. Based on the log-determinant heuristic λ_{LT} is given by

$$\lambda_{LT}^i = \lambda_L g_l(\sigma_i^t) = \lambda_L g_{\log}(\sigma_i^t) = \frac{\lambda_L}{(\gamma + \sigma_i^t)}, \forall i. \quad (38)$$

Based on the exponential decay heuristic λ_{LT} is given by

$$\lambda_{LT}^i = \lambda_L g_l(\sigma_i^t) = \lambda_L g_{\exp}(\sigma_i^t) = \frac{\lambda_L}{\gamma} \exp\left(\frac{-\sigma_i^t}{\gamma}\right). \quad (39)$$

Here, σ_i^t is the i -th singular value of the t -th estimate of \mathbf{L} , i.e., $(\mathbf{L})^t$.

III. UNFOLDING ADMM BASED LOW-RANK PLUS SPARSE RECOVERY ALGORITHM

In this section, we are going to discuss the ADMM algorithm unfolding using a deep neural network (DNN). First, in the following, we summarize the three main ADMM steps which are used to solve the low-rank plus sparse problem given in (8),

$$(\mathbf{L})^{t+1} = \text{SVT}_{\boldsymbol{\lambda}_{LT}} \left(\mathbf{A}_l^\dagger \left(\mathbf{y} - \mathbf{A}_s \text{vec}((\mathbf{S})^t) + \frac{1}{\rho}(\mathbf{u})^t \right) \right), \quad (40)$$

$$(\mathbf{S})^{t+1} = \text{ST}_{\lambda_{ST}} \left(\mathbf{A}_s^\dagger \left(\mathbf{y} - \mathbf{A}_l \text{vec}((\mathbf{L})^{t+1}) + \frac{1}{\rho}(\mathbf{u})^t \right) \right), \quad (41)$$

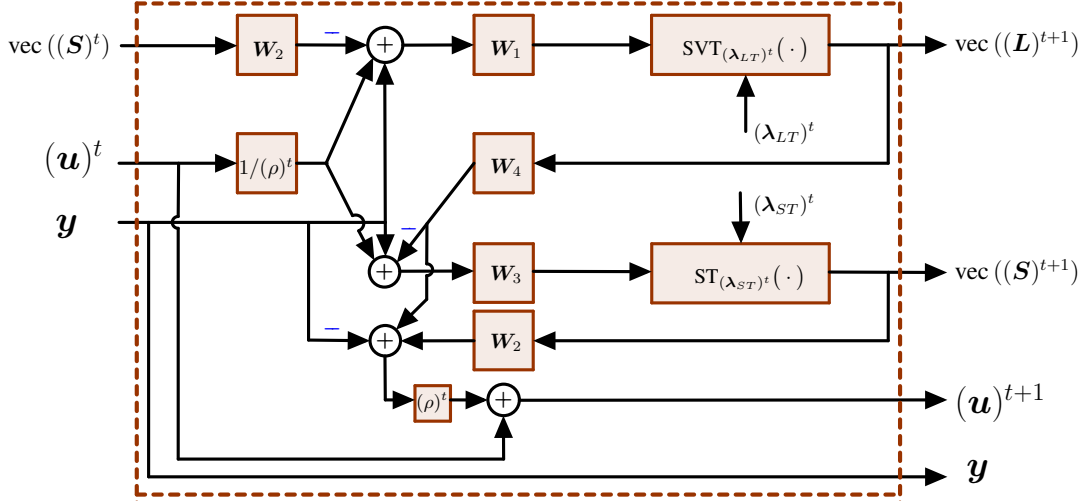


Fig. 2. Block diagram of the single layer (t -th layer) of the DNN which mimic the low-rank plus recovery algorithm 1.

Algorithm 1: Low-rank-plus-sparse recovery algorithm

Input: \mathbf{y} , $\epsilon = 10^{-6}$, max iterations (J), \mathbf{A}_l , \mathbf{A}_s .

Initialization: $\rho = 10^{-2}$, $\rho_o = 1.001$, $t = 0$,

$(\mathbf{L})^0 = \text{vec}^{-1}(\mathbf{A}_l^\dagger \mathbf{y})$, $(\mathbf{S})^0 = \mathbf{0}_{M,N}$, $(\mathbf{u})^0 = \mathbf{0}_K$.

while $\|\mathbf{A}_l \text{vec}(\mathbf{L}) + \mathbf{A}_s \text{vec}(\mathbf{S}) - \mathbf{y}\|_2^2 > \epsilon$ or $t < T$ **do**

ADMM step 1: Update L

Update λ_{LT} by (38), then estimate \mathbf{L} by,

$$(\mathbf{L})^{t+1} = \text{SVT}_{\lambda_{LT}} \left(\mathbf{A}_l^* \left(\mathbf{y} - \mathbf{A}_s \text{vec}((\mathbf{S})^t) + \frac{1}{\rho} (\mathbf{u})^t \right) \right).$$

ADMM step 2: Update S

Update λ_{ST} by (32), then estimate \mathbf{S} by,

$$(\mathbf{S})^{t+1} = \text{ST}_{\lambda_{ST}} \left(\mathbf{A}_s^* \left(\mathbf{y} - \mathbf{A}_l \text{vec}((\mathbf{L})^{t+1}) + \frac{1}{\rho} (\mathbf{u})^t \right) \right).$$

ADMM step 3: Update u, ρ and t

Update $(\mathbf{u})^{t+1}$ by

$$(\mathbf{u})^{t+1} = (\mathbf{u})^t + \rho \left(\mathbf{A}_s \text{vec}((\mathbf{S})^{t+1}) + \mathbf{A}_l \text{vec}((\mathbf{L})^{t+1}) - \mathbf{y} \right).$$

$\rho = \min(\rho_o \times \rho, \rho_m)$, and $t = t + 1$.

$\mathbf{L} \leftarrow \mathbf{L}^{t+1}$ and $\mathbf{S} \leftarrow \mathbf{S}^{t+1}$.

Output: \mathbf{L} , \mathbf{S} .

$$(\mathbf{u})^{t+1} = (\mathbf{u})^t + \rho \left(\mathbf{A}_s \text{vec}((\mathbf{S})^{t+1}) + \mathbf{A}_l \text{vec}((\mathbf{L})^{t+1}) - \mathbf{y} \right). \quad (42)$$

An iterative algorithm given in algorithm 1 utilizes a sequence of steps to estimate the solution based on the ADMM steps given in (40), (41) and (42). Here, previous estimates are used in the next iteration. Thus, this kind of iterative algorithm can be considered as a recurrent neural network. The t -th iteration of the iterative algorithm is modeled as the t -th layer of the deep neural network. Each matrix multiplication given in the ADMM steps (40), (41) and (42) is considered as the weights of the deep neural network. Here, our main objective is to learn the weights of the deep neural network and thresholding

parameters λ_S and λ_L given in (32) and (38) from the training data. To this end, the t -th layer of the neural network is represented by the following equations.

$$(\mathbf{L})^{t+1} = \text{SVT}_{(\lambda_{LT})^t} \left(\mathbf{W}_1 \left(\mathbf{y} - \mathbf{W}_2 \text{vec}((\mathbf{S})^t) + \frac{1}{(\rho)^t} (\mathbf{u})^t \right) \right), \quad (43)$$

$$(\mathbf{S})^{t+1} = \text{ST}_{(\lambda_{ST})^t} \left(\mathbf{W}_3 \left(\mathbf{y} - \mathbf{W}_4 \text{vec}((\mathbf{L})^{t+1}) + \frac{1}{(\rho)^t} (\mathbf{u})^t \right) \right), \quad (44)$$

$$(\mathbf{u})^{t+1} = (\mathbf{u})^t + (\rho)^t \left(\mathbf{W}_2 \text{vec}((\mathbf{S})^t) + \mathbf{W}_4 \text{vec}((\mathbf{L})^{t+1}) - \mathbf{y} \right). \quad (45)$$

Here, \mathbf{W}_1 , \mathbf{W}_2 , \mathbf{W}_3 and \mathbf{W}_4 are the weights of the t -th layer of the deep neural network as shown in Fig. 2, their initial values are $\mathbf{W}_1 = \mathbf{A}_l^*$, $\mathbf{W}_2 = \mathbf{A}_s$, $\mathbf{W}_3 = \mathbf{A}_s^*$ and $\mathbf{W}_4 = \mathbf{A}_l$ to mimic the ADMM algorithm given in algorithm 1. Further, $(\lambda_{LT})^t$ and $(\lambda_{ST})^t$ are the thresholding parameters of the t -th layer, which are calculated as given in (32) and (38). Note that, $(\lambda_{LT})^t$ and $(\lambda_{ST})^t$ depend on the previous estimates of the $(\mathbf{L})^t$, $(\mathbf{S})^t$ and two parameters (λ_S and λ_L). Here, we consider matrices \mathbf{W}_1 , \mathbf{W}_2 , \mathbf{W}_3 and \mathbf{W}_4 are tied over all the layers, i.e., sharing weights. However, we do not consider thresholding parameters (λ_S and λ_L) and γ to be tied over all layers, i.e., each layer has its own thresholding parameters. To this end, $\Theta = \left\{ \lambda_S^{(t)}, \lambda_L^{(t)}, \gamma^{(t)}, (\rho)^t, \mathbf{W}_1, \mathbf{W}_2, \mathbf{W}_3, \mathbf{W}_4 \right\}$

represents the set of learning parameters. Here, $\lambda_S^{(t)}$ and $\lambda_L^{(t)}$ are the thresholding parameters of the t -th layer. The unfolded architecture of the low-rank plus sparse recovery algorithm 1 is shown in Fig. 2. Here, this figure shows a single layer of the deep neural network (t -th layer) and this layer is equivalent to the t -th iteration of algorithm 1.

A. Training phase

In the training phase, the DNN is trained in a supervised manner. Here, the DNN learns the parameters given in $\Theta = \left\{ \lambda_S^{(t)}, \lambda_L^{(t)}, \gamma^{(t)}, (\rho)^t, \mathbf{W}_1, \mathbf{W}_2, \mathbf{W}_3, \mathbf{W}_4 \right\}$. Suppose that the DNN has T layers, then the outputs of the DNN in the training phase for the i -th sample are given by $(\mathbf{L}_i)^T$ and

$(\mathbf{S}_i)^T$, respectively. Note that, in the training phase, the DNN minimizes the normalized mean squared error

$$\text{MSE} = \frac{1}{T_s} \sum_{i=1}^{T_s} \left(\frac{1}{2} \frac{\|(\mathbf{L}_i)^T - \mathbf{L}_i\|_F^2}{\|\mathbf{L}_i\|_F^2} + \frac{1}{2} \frac{\|(\mathbf{S}_i)^T - \mathbf{S}_i\|_F^2}{\|\mathbf{S}_i\|_F^2} \right), \quad (46)$$

where \mathbf{S}_i and \mathbf{L}_i are i -th ground-truth low rank and sparse matrices and T_s is the number of training samples.

In this work, we consider three versions of the proposed DNN based ADMM thresholding as follows. (a) Parameter learning with non adaptive thresholding. Here, we consider $G_s(\theta) = G_l(\theta) = |\theta|$ and $g_s(\theta) = g_l(\theta) = 1$ and this approach is named as ADMM based trained robust principal component analysis (RPCA) with thresholding (TRPCA-T). For the parameter learning with adaptive thresholding, we consider two versions based on two surrogate functions (logarithm and exponential) as described in II-C and II-D. These two approaches are named as follows. (b) ADMM based trained RPCA with adaptive thresholding based on logarithm heuristic (TRPCA-AT(log)). (c) ADMM based trained RPCA with adaptive thresholding based on exponential heuristic (TRPCA-AT(exp)).

B. Trained vs. untrained recovery

To have a comparison with the deep learning-based trained ADMM adaptive thresholding, we consider two approaches. In the first approach, we consider the untrained ADMM approach to solve the low-rank plus sparse recovery as given in algorithm 1 with $G_s(\theta) = G_l(\theta) = |\theta|$ (i.e., by using the ℓ_1 norm and nuclear norm). This method is named as ADMM based untrained RPCA with thresholding (URPCA-T). As a second option, we consider the convex relaxation of the low-rank plus sparse recovery problem given in (8) as follows.

$$\begin{aligned} \left\{ \hat{\mathbf{L}}, \hat{\mathbf{S}} \right\} &= \arg \min_{\mathbf{L}, \mathbf{S}} \lambda_l \|\mathbf{L}\|_* + \lambda_s \|\mathbf{S}\|_1, \\ \text{s.t. } \|\mathbf{y} - \mathbf{A} \text{vec}(\mathbf{S}) - \mathbf{A} \text{vec}(\mathbf{L})\|_2^2 &\leq \epsilon. \end{aligned} \quad (47)$$

Here, λ_l , λ_s are regularization parameters and ϵ is a small positive constant (noise bound). This method is named as low-rank plus sparse recovery with convex relaxation (LRPSRC). Next, we validate the proposed DNN based low-rank plus sparse recovery unfolding numerically.

IV. SIMULATION RESULTS

In this section numerical results are presented. First, the performance of deep learning-based trained ADMM adaptive thresholding is evaluated with a generic real-valued Gaussian model and next a complex-valued SFCW radar model given in Section II-A is used.

A. Generic Gaussian model

Here, the elements of the matrix $\mathbf{A}_l = \mathbf{A}_s = \mathbf{A} \in \mathbb{R}^{K \times MN}$ are generated from an i.i.d. Gaussian distribution with zero mean and variance 1. The rank of the ground-truth low-rank matrix \mathbf{L} is set to 2 and the number of non-zero elements of the ground-truth sparse matrix \mathbf{S} is set as 5. \mathbf{y} is generated based on the (7) and the signal-to-noise ratio is SNR :=

$\|\text{Avec}(\mathbf{L}) + \text{Avec}(\mathbf{S})\|_2^2 / \|\mathbf{n}\|_2^2 = 20\text{dB}$ and $M = 30$, $N = 30$. Further, we normalized the matrices \mathbf{S} and \mathbf{L} to have a unit Frobenius norm (i.e., $\|\mathbf{L}\|_F^2 = \|\mathbf{S}\|_F^2 = 1$). Generally, many training samples are required to train a deep neural network. However, due to the specific architecture of the iterative algorithm, here we are able to train the DNN with a small data set of 500 samples for the Gaussian model. In the training phase, the adaptive moment estimation (Adam) optimizer [57] with a learning rate of 0.1 is used to train the DNN and batch size was set as 50. Note that, in the Gaussian model, the DNN only learns the $\lambda_S^{(t)}$ and $\lambda_L^{(t)}$ instead of all the parameters given in $\Theta = \left\{ \lambda_S^{(t)}, \lambda_L^{(t)}, \gamma^{(t)}, (\rho)^t, \mathbf{W}_1, \mathbf{W}_2, \mathbf{W}_3, \mathbf{W}_4 \right\}$. Here, we set $\mathbf{W}_1 = \mathbf{A}_l^\dagger$, $\mathbf{W}_2 = \mathbf{A}_s$, $\mathbf{W}_3 = \mathbf{A}_s^\dagger$ and $\mathbf{W}_4 = \mathbf{A}_l$ to mimic the ADMM algorithm given in algorithm 1 and $\gamma = 1$. In the training phase, the DNN is trained over a maximum of 500 epochs.

In the inference phase, to evaluate the performance of the DNN, the normalized average mean squared error is used. For low-rank and sparse matrix it is given by

$$\text{MSE}_L = \frac{1}{N_s} \sum_{i=1}^{N_s} \left(\frac{\|(\mathbf{L}_i)^T - \mathbf{L}_i\|_F^2}{\|\mathbf{L}_i\|_F^2} \right), \quad (48)$$

$$\text{MSE}_S = \frac{1}{N_s} \sum_{i=1}^{N_s} \left(\frac{\|(\mathbf{S}_i)^T - \mathbf{S}_i\|_F^2}{\|\mathbf{S}_i\|_F^2} \right). \quad (49)$$

The outputs of a DNN with T layers is for the i -th testing sample are given by $(\mathbf{S}_i)^T$ and $(\mathbf{L}_i)^T$, respectively. Here, \mathbf{S}_i and \mathbf{L}_i are i -th ground-truth low rank and sparse matrices and $N_s = 1200$ is the number of testing samples. The performance of the proposed ADMM based trained RPCA with adaptive thresholding is compared with algorithm 1 (i.e., ADMM based untrained RPCA with thresholding (URPCA-T)) and the solution of the standard convex relaxation of the low-rank plus recovery problem given in (47) (LRPSRC). Both algorithm 1 and (47) are implemented using the Matlab [58] and (47) is solved using the CVX package [59]. Notice that, in the LRPSRC λ_l and λ_s are set to 1, and $1/\sqrt{\max(M, N)}$, respectively as suggested by [22]. Note that for algorithm 1, there is no specific rule to select the λ_L and λ_S and ρ , therefore they are manually tuned based on the data¹. As an example for the Gaussian data with 50% compression ratio ($K/MN = 50\%$), we set $\lambda_L = 0.15/\rho$ and $\lambda_S = 0.4/(\rho \sqrt{\max(M, N)})$ in algorithm 1 and the ADMM auxiliary parameter ρ is initialized as 0.01 and after each iteration ρ is increased by a small factor $\rho_m = 1.001$ as suggested by [35]. The DNN is implemented using the Pytorch package [60].

The average normalized MSEs for the different number of layers of the DNN are for compression ratio (K/MN) 50% and 25% shown in Figs. 3 and 4, respectively. Figs. 3 and 4 show that the proposed DNN based thresholding (TRPCA-AT(log) and TRPCA-AT(exp)) outperforms the URPCA-T and the LRPSRC. Further, it is observed that as the number of layers increases the average MSE decreases. For the 50%

¹When \mathbf{A} is identity matrix, there is a specific rule to select λ_S as $1/\sqrt{\max(M, N)}$ [22]

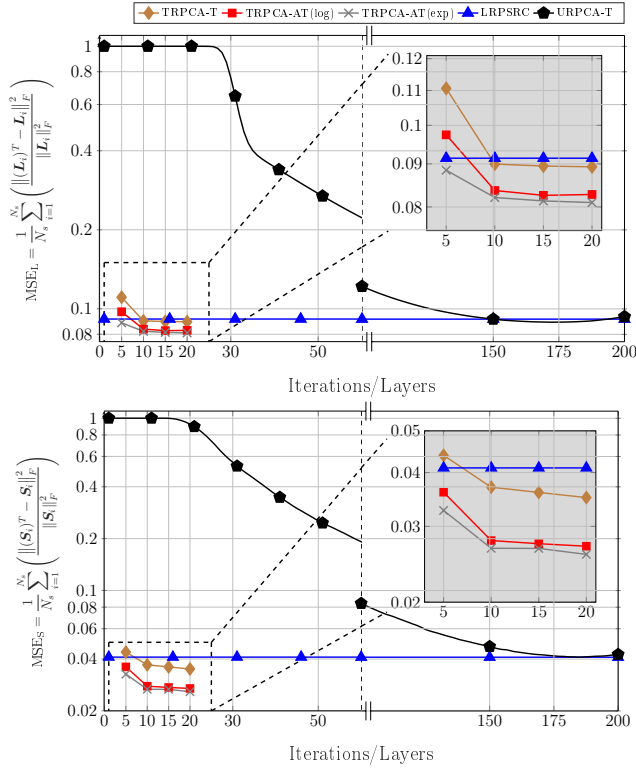


Fig. 3. Average recovery error of low-rank (top) and sparsity (bottom) contributions compression ratio $K/MN = 50\%$.

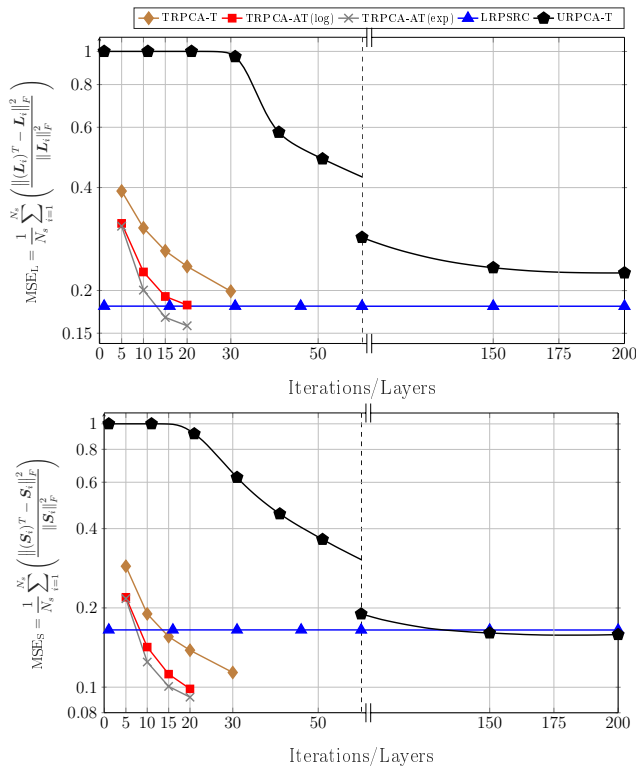


Fig. 4. Average recovery error of low-rank (top) and sparsity (bottom) contributions for compression ratio $K/MN = 25\%$.

compressing ratio, the average MSE does not show a large variance after ten layers. However, for the 25% compressing

ratio this is not the case. This is due to the fact that, as the compression ratio increases recovering of the low-rank and the sparse matrix become more challenging. Thus, for a harder problem adding more layers shows noticeable improvement compared to an easy problem.

Further, the TRPCA-AT outperforms the TRPCA-T. This performance improvement is mainly due to the iterative reweighting of ℓ_1 -norm and nuclear norm minimization. Also, the improvement over non-weighting to iterative reweighting is more visible as the compression ratio increases (i.e., as the problem getting more challenging). As an example, for the 25% compressing ratio, the average MSE improvement between the TRPCA-T with twenty layers and TRPCA-AT (exp) with twenty layers for the low-rank and sparse components are 32.93% and 50.77%, respectively. However, for the 50% compressing ratio, this improvement for the low-rank and sparse components are 9.31% and 26.21%, respectively. Further, we observe slight performance gains as the concave surrogate is changed from log-determinant to exponential. As we compare the number of layers of the TRPCA-AT to the number of iterations of the URPCA-T, the TRPCA-AT achieves 1 : 20 improvement. In more details, TRPCA-AT with ten layers outperforms URPCA-T with 200 iterations. Therefore, in the testing phase (inference phase), our proposed approach (TRPCA-AT) is twenty times faster than the conventional untrained approach (URPCA-T). Besides, Figs. 3 and 4 demonstrate the singular value and soft thresholding based URPCA-T converges to the MSE of the convex relaxation of the low-rank plus sparse recovery problem given in (47) (LRPSRC).

B. SFCW radar model

In this subsection, the performance evaluation of the ADMM based trained RPCA with adaptive thresholding was performed based on the SFCW radar model given in Section II-A. In the simulations, we set the carrier frequency f_c of 300 GHz and bandwidth B as 5 GHz. Further, both N and M are set as 30. The inter-antenna spacing is chosen as half of the wavelength of f_c . Here, we consider a single-layered structure and the distance to the front surface of the layered structure is 1.0 m. Both height and length of the layered structure is 0.5 m. In the simulations, we consider six defects and the scene is partitioned into a 16×16 grid with equal grid size (i.e., $Q = 256$). The grid size is selected according to the Rayleigh resolution of the radar. In the simulations, the signal-to-noise ratio is $SNR := \frac{\|\Phi \text{vec}(\mathbf{Y}^l) + \Phi \mathbf{D} \mathbf{s}\|_2^2}{\|\Phi \text{vec}(\mathbf{Z})\|_F^2} = 20\text{dB}$. Note that based on numerical results we slightly adjust the λ_S and λ_L of the algorithm 1 as $\lambda_L = 0.25/\rho$ and $\lambda_S = 0.25/(\rho \sqrt{\max(M, N)})$.

Note that the SFCW data consists of complex numbers, therefore, in this work, we implemented the DNN which supports complex numbers². Similar to the generic Gaussian model, we tested the performance of the our proposed approach for the different number of layers of the DNN. More specifically we

²In this work, we used the pytorch version 1.8.1 to implement the DNN. This version supports complex numbers and also it supports back-propagation through singular value decomposition of a complex valued matrix.

change the number of layers of the DNN from 5 to 30 by step of 5.

Interestingly, in contrast to the generic Gaussian model only learning the $\lambda_S^{(t)}$ and $\lambda_L^{(t)}$ does not achieve satisfactory average MSEs of the low-rank and sparse components. We believe this is due to the fact that, the estimation of \mathbf{Y}^l and \mathbf{s} from the \mathbf{y}_{cs} given in (6) is more challenging than the Gaussian model given in (7). Therefore, we enable learning all parameters given in $\Theta = \{\lambda_S^{(t)}, \lambda_L^{(t)}, \gamma^{(t)}, (\rho)^t, \mathbf{W}_1, \mathbf{W}_2, \mathbf{W}_3, \mathbf{W}_4\}$. Further, we notice that the stochastic gradient descent (SGD) optimizer [61], [62] performs better than the Adam optimizer in learning the weights of the DNN ($\mathbf{W}_1, \mathbf{W}_2, \mathbf{W}_3$ and \mathbf{W}_4) and other parameters ($\lambda_S^{(t)}, \lambda_L^{(t)}, \gamma^{(t)}, (\rho)^t$) together. Therefore, we consider a three-stage training process to achieve better learning.

In the first stage, we only learn the $\lambda_S^{(t)}$ and $\lambda_L^{(t)}$ for 50 epochs using the Adam optimizer. In the second stage, we learn all parameters given in Θ using the SGD optimizer for 50 epochs. Finally, we only learn the $\lambda_S^{(t)}$ and $\lambda_L^{(t)}$ for 15 epochs using the Adam optimizer. Also, we slightly adjusted the learning rate as the number of layers of the DNN increases. For the first stage, we employed learning rates 1×10^{-1} , 5×10^{-2} and 5×10^{-3} for the DNN with 5/10, 15/20 and 25/30 layers, respectively. Here, only exception is the TRPCA-T. For the TRPCA-T, we consider the learning rate of 5×10^{-2} for the DNN with 25/30 layers as well. This is due to the fact that, we observe that the non adaptive thresholding based approach TRPCA-T is less sensitive to the change of parameters compared to the adaptive thresholding based approaches TRPCA-AT. For the second stage, we employed the learning rate as 1×10^{-3} for all layers combinations of the DNN. For the third stage, we consider learning rates 2.5×10^{-4} for the for all layers combinations of the DNN. Note that, in the final training stage, similar to the Gaussian model, we only learn the $\lambda_S^{(t)}$ and $\lambda_L^{(t)}$. The main reason to consider the final training is that, it achieves higher performance gains with respect to continuation of the second step for another 15 epochs. Also, note that there is a specific reason to use the first stage without directly using the second stage. This is due to the unbalance of \mathbf{A}_s and \mathbf{A}_l of the SFCW model compared to the generic Gaussian model. Note that, $\mathbf{A}_s = \Phi \mathbf{D}$ and $\mathbf{A}_l = \Phi$. More specifically, $\mathbf{A}_l = \Phi$ and Φ is the selection matrix (as described in Section II-B). This matrix has a single non-zero element of value 1 in each row to indicate the selected frequency of a particular antenna if that antenna is selected. However, $\mathbf{A}_s = \Phi \mathbf{D}$ so, \mathbf{A}_s is a combination of the selection matrix and the matrix \mathbf{D} . Note that, the matrix \mathbf{D} is generated based on the time delays of the grid (as described in Section II-A). Therefore, the matrix \mathbf{A}_s contains more information compared to the matrix \mathbf{A}_l . Therefore, \mathbf{A}_s is more difficult to learn compared to \mathbf{A}_l . This results in an imbalance in the training phase if we directly start with the stage two. That means the MSE of the low-rank component tends to be much smaller compared to the MSE of the sparse component in the training phase if we directly start with the second stage.

In the defect detection by SFCW radar, we consider a data set of 600 samples. Here, 500 data samples are used for training

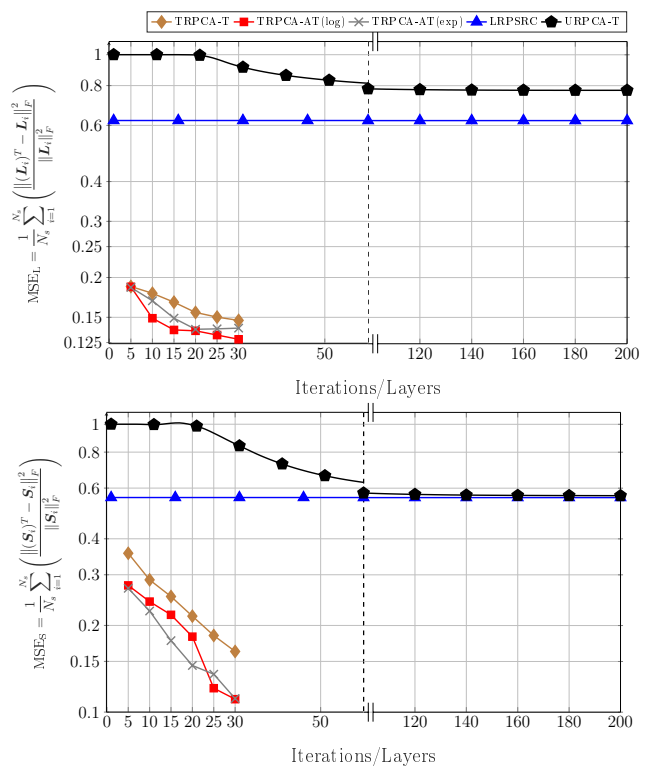


Fig. 5. Average recovery error of low-rank (top) and sparsity (bottom) contributions for compression ratio $K/MN = 20\%$.

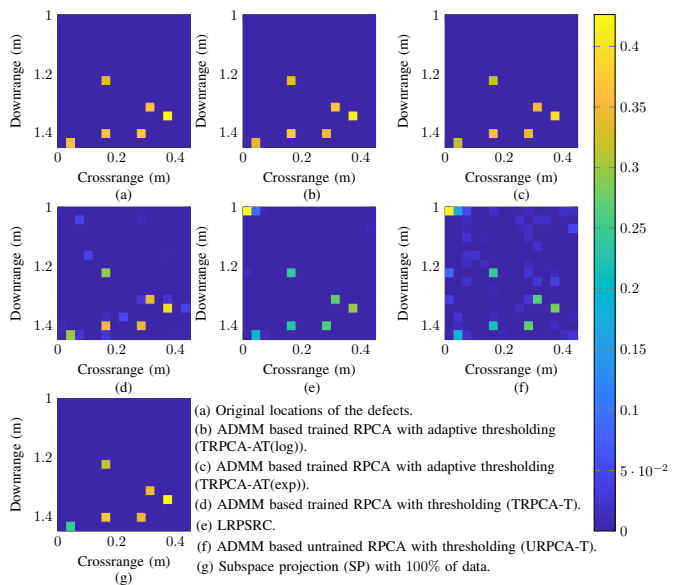


Fig. 6. Object recovery in single case for compression ratio $K/MN = 20\%$

and validation and 100 data samples are used for testing. Here, we used Matlab [58] to generate the SFCW data based on the system model given in (6).

The average normalized MSEs for the different numbers of layers of the DNN for the compression ratio (K/MN) 20% is shown in Fig. 5. The figure shows that the proposed TRPCA-AT outperforms both URPCA-T and the LRPSRC given in (47). Further, in terms of the average MSE, the TRPCA-AT

and TRPCA-T with five layers outperform URPCA-T with 200 iterations. Therefore, as we compare the number of layers of the TRPCA-AT to the number of iterations of the URPCA-T, the TRPCA-AT achieves a 1 : 40 improvement for the SFCW radar data, i.e., our proposed approach (TRPCA-AT) is forty times faster than the conventional untrained approach (URPCA-T). Moreover, based on the results shown in Fig. 5, the TRPCA-AT shows better performance compared to the TRPCA-T. Also, note that with a 20% of compression ratio, the estimation of Y^l and s from y_{cs} in (6) is more challenging. Therefore, the average MSE of the LRPSRC is higher than 0.5. However, the DNN based TRPCA-AT is able to achieve average MSE in the range of 0.1 for both sparse and the low-rank components Y^l .

Next, to further illustrate the defect detection, an image of the recovered detects are formed. Here, the recovered vector s is reshaped into a matrix to obtain an image of the detects as shown in Fig. 6 for a single data sample. As a benchmark here we consider the state-of-the-art subspace projection (SP) [10] method with the full data set (i.e., compression ratio $(K/MN) = 100\%$). Further, for SP, it is assumed that the number of defects is known. Fig. 6 (a) shows the actual defect locations. The recovered locations of the defects for the ADMM based trained RPCA with adaptive thresholding based on logarithm heuristic (TRPCA-AT(log)), ADMM based trained RPCA with adaptive thresholding based on exponential heuristic (TRPCA-AT(exp)), ADMM based trained RPCA with thresholding (TRPCA-T), the LRPSRC, ADMM based untrained RPCA with thresholding (URPCA-T) and the SP are shown in (b), (c), (d), (e), (f) and (g), respectively. It can be seen that the proposed TRPCA-AT approaches are able to identify all six defects.

Further, the proposed TRPCA-AT approaches are able to estimate amplitudes of the recovered defects (s vector) closer to the actual defects. Therefore, it is observed that defect detection with the proposed TRPCA-AT approaches outperform state-of-the-art SP even with 20% of data.

V. CONCLUSION

This paper presents a deep learning-based low-rank plus sparse recovery approach for the detection of material defects based on compressive sensing. To this end, an iterative algorithm is developed based on ADMM to estimate the low-rank and sparse contributions with the iterative reweighted nuclear and ℓ_1 -norm minimization. In particular, we propose deep learning based algorithm unfolding to improve the accuracies of the recovered low-rank and sparse components and the speed of convergence of the algorithm. The results show that, the deep learning based algorithm unfolding performs substantially better compared to the untrained iterative algorithm in terms of low-rank and sparse component recovery and convergence speed. In addition to that, it is observed that as the compression ratio increases, the improvement with deep learning becomes more visible.

REFERENCES

- [1] S. Gholizadeh, "A review of non-destructive testing methods of composite materials," *Procedia Structural Integrity*, vol. 1, pp. 50–57, 2016.
- [2] P. Hillger, M. van Delden, U. S. M. Thantrige, A. M. Ahmed, J. Witte-meier, K. Arzi, M. Andree, B. Sievert, W. Prost, A. Rennings, D. Erni, T. Musch, N. Weimann, A. Sezgin, N. Pohl, and U. R. Pfeiffer, "Toward mobile integrated electronic systems at THz frequencies," *Journal of Infrared, Millimeter, and Terahertz Waves*, vol. 41, no. 7, pp. 846–869, 2020.
- [3] C. Baker, T. Lo, W. R. Tribe, B. E. Cole, M. R. Hogbin, and M. C. Kemp, "Detection of concealed explosives at a distance using Terahertz technology," *Proc. IEEE*, vol. 95, no. 8, pp. 1559–1565, 2007.
- [4] Y. S. Yoon and M. G. Amin, "Spatial filtering for wall-clutter mitigation in through-the-wall radar imaging," *IEEE Trans. on Geosci. and Remote Sens.*, vol. 47, no. 9, pp. 3192–3208, 2009.
- [5] A. Kariminezhad and A. Sezgin, "Spatio-temporal waveform design in active sensing systems with multilayer targets," *EUSIPCO*, pp. 1–5, 2019.
- [6] U. S. K. P. M. Thantrige, J. Barowski, I. Rolfes, D. Erni, T. Kaiser, and A. Sezgin, "Characterization of dielectric materials by sparse signal processing with iterative dictionary updates," *IEEE Sens. Lett.*, vol. 4, no. 9, pp. 1–4, 2020.
- [7] C. D. Stoik, M. J. Bohn, and J. L. Blackshire, "Nondestructive evaluation of aircraft composites using transmissive Terahertz time domain spectroscopy," *Optics express*, vol. 16, no. 21, pp. 17 039–17 051, 2008.
- [8] F. H. C. Tivive, A. Bouzerdoum, and M. G. Amin, "An SVD-based approach for mitigating wall reflections in through-the-wall radar imaging," *2011 IEEE Radar Conf.*, pp. 519–524, 2011.
- [9] —, "A subspace projection approach for wall clutter mitigation in through-the-wall radar imaging," *IEEE Trans. on Geosci. and Remote Sens.*, vol. 53, no. 4, pp. 2108–2122, 2014.
- [10] U. S. Khan and W. Al-Nuaimy, "Background removal from GPR data using eigenvalues," *Proc. of the XIII Int. Conf. on Ground Penetrating Radar*, pp. 1–5, 2010.
- [11] D. L. Donoho, "Compressed sensing," *IEEE Trans. Inf. Theory*, vol. 52, no. 4, pp. 1289–1306, 2006.
- [12] V. H. Tang, A. Bouzerdoum, S. L. Phung, and F. H. C. Tivive, "Enhanced wall clutter mitigation for compressed through-the-wall radar imaging using joint bayesian sparse signal recovery," *ICASSP*, pp. 7804–7808, 2014.
- [13] —, "Indoor scene reconstruction for through-the-wall radar imaging using low-rank and sparsity constraints," *2016 IEEE Radar Conf.*, pp. 1–4, 2016.
- [14] A. Bouzerdoum, V. H. Tang, and S. L. Phung, "A low-rank and jointly-sparse approach for multipolarization through-wall radar imaging," *2017 IEEE Radar Conf.*, pp. 0263–0268, 2017.
- [15] V. H. Tang, A. Bouzerdoum, S. L. Phung, and F. H. C. Tivive, "Radar imaging of stationary indoor targets using joint low-rank and sparsity constraints," *ICASSP*, pp. 1412–1416, 2016.
- [16] Q. Huang, L. Qu, B. Wu, and G. Fang, "UWB through-wall imaging based on compressive sensing," *IEEE Trans. on Geosci. and Remote Sensing*, vol. 48, no. 3, pp. 1408–1415, 2009.
- [17] Y. S. Yoon and M. G. Amin, "Through-the-wall radar imaging using compressive sensing along temporal frequency domain," *ICASSP*, pp. 2806–2809, 2010.
- [18] V. H. Tang, A. Bouzerdoum, and S. L. Phung, "Multipolarization through-wall radar imaging using low-rank and jointly-sparse representations," *IEEE Trans. on Image Process.*, vol. 27, no. 4, pp. 1763–1776, 2018.
- [19] T. Van Ha, A. Bouzerdoum, and S. L. Phung, "A matrix completion approach for wall-clutter mitigation in compressive radar imaging of indoor targets," in *ICASSP*, 2018, pp. 1608–1612.
- [20] J. Wang, G. Xu, C. Li, Z. Wang, and F. Yan, "Surface defects detection using non-convex total variation regularized RPCA with kernelization," *IEEE Trans. Instrum. Meas.*, vol. 70, pp. 1–13, 2021.
- [21] D. Mo, W. K. Wong, Z. Lai, and J. Zhou, "Weighted double-low-rank decomposition with application to fabric defect detection," *IEEE Trans. Autom. Sci. Eng.*, pp. 1–21, 2020.
- [22] E. J. Candès, X. Li, Y. Ma, and J. Wright, "Robust principal component analysis?" *Journal of the ACM*, vol. 58, no. 3, pp. 1–37, 2011.
- [23] X. Yuan and J. Yang, "Sparse and low-rank matrix decomposition via alternating direction methods," *Preprint*, vol. 12, no. 2, 2009.
- [24] J. A. Tropp, "Just relax: convex programming methods for identifying sparse signals in noise," *IEEE Trans. Inf. Theory*, vol. 52, no. 3, pp. 1030–1051, 2006.
- [25] A. M. Bruckstein, D. L. Donoho, and M. Elad, "From sparse solutions of systems of equations to sparse modeling of signals and images," *SIAM Review*, vol. 51, no. 1, pp. 34–81, 2009.

- [26] E. J. Candes, J. K. Romberg, and T. Tao, "Stable signal recovery from incomplete and inaccurate measurements," *Communications on Pure and Applied Mathematics: A Journal Issued by the Courant Institute of Mathematical Sciences*, vol. 59, no. 8, pp. 1207–1223, 2006.
- [27] E. J. Candès and B. Recht, "Exact matrix completion via convex optimization," *Foundations of Computational Mathematics*, vol. 9, no. 6, pp. 717–772, 2009.
- [28] J. Cai, E. J. Candès, and Z. Shen, "A singular value thresholding algorithm for matrix completion," *SIAM Journal on Optimization*, vol. 20, no. 4, pp. 1956–1982, 2010.
- [29] M. Fazel, H. Hindi, and S. P. Boyd, "A rank minimization heuristic with application to minimum order system approximation," in *Proceedings of the 2001 American Control Conf.*, vol. 6. IEEE, 2001, pp. 4734–4739.
- [30] E. J. Candes and T. Tao, "The power of convex relaxation: Near-optimal matrix completion," *IEEE Trans. Inf. Theory*, vol. 56, no. 5, pp. 2053–2080, 2010.
- [31] E. J. Candes, M. B. Wakin, and S. P. Boyd, "Enhancing sparsity by reweighted ℓ_1 minimization," *Journal of Fourier analysis and Applications*, vol. 14, no. 5-6, pp. 877–905, 2008.
- [32] I. Daubechies, R. DeVore, M. Fornasier, and C. S. Güntürk, "Iteratively reweighted least squares minimization for sparse recovery," *Communications on Pure and Applied Mathematics: A Journal Issued by the Courant Institute of Mathematical Sciences*, vol. 63, no. 1, pp. 1–38, 2010.
- [33] K. Mohan and M. Fazel, "Reweighted Nuclear norm minimization with application to system identification," in *Proc. of the 2010 American Control Conf.* IEEE, 2010, pp. 2953–2959.
- [34] S. Gu, Q. Xie, D. Meng, W. Zuo, X. Feng, and L. Zhang, "Weighted Nuclear norm minimization and its applications to low level vision," *Int. Journal of Comput. Vision*, vol. 121, no. 2, pp. 183–208, 2017.
- [35] C. Lu, J. Feng, S. Yan, and Z. Lin, "A unified alternating direction method of multipliers by majorization minimization," *IEEE Trans. Pattern Anal. Mach. Intell.*, vol. 40, no. 3, pp. 527–541, 2018.
- [36] K. Gregor and Y. LeCun, "Learning fast approximations of sparse coding," in *Proceedings of the 27th int. Conf. on Machine Learning*, 2010, pp. 399–406.
- [37] D. Kim and D. Park, "Element-wise adaptive thresholds for learned iterative shrinkage thresholding algorithms," *IEEE Access*, vol. 8, pp. 45 874–45 886, 2020.
- [38] Y. Yang, J. Sun, H. Li, and Z. Xu, "ADMM-CSNet: A deep learning approach for image compressive sensing," *IEEE Trans. Pattern Anal. Mach. Intell.*, vol. 42, no. 3, pp. 521–538, 2020.
- [39] S. Lohit, D. Liu, H. Mansour, and P. T. Boufounos, "Unrolled projected gradient descent for multi-spectral image fusion," in *ICASSP*, 2019, pp. 7725–7729.
- [40] Y. Li, M. Tofighi, J. Geng, V. Monga, and Y. C. Eldar, "Efficient and interpretable deep blind image deblurring via algorithm unrolling," *IEEE Trans. Comput. Imag.*, vol. 6, pp. 666–681, 2020.
- [41] G. Dardikman-Yoffe and Y. C. Eldar, "Learned SPARCOM: unfolded deep super-resolution microscopy," *Optics Express*, vol. 28, no. 19, pp. 27 736–27 763, 2020.
- [42] R. Cohen, Y. Zhang, O. Solomon, D. Toberman, L. Taieb, R. J. van Sloun, and Y. C. Eldar, "Deep convolutional robust PCA with application to ultrasound imaging," in *ICASSP*, 2019, pp. 3212–3216.
- [43] O. Solomon, R. Cohen, Y. Zhang, Y. Yang, Q. He, J. Luo, R. J. G. van Sloun, and Y. C. Eldar, "Deep unfolded robust PCA with application to clutter suppression in ultrasound," *IEEE Trans. Med. Imag.*, vol. 39, no. 4, pp. 1051–1063, 2020.
- [44] V. Monga, Y. Li, and Y. C. Eldar, "Algorithm unrolling: Interpretable, efficient deep learning for signal and image processing," *IEEE Signal Process. Magazine*, vol. 38, no. 2, pp. 18–44, 2021.
- [45] R. J. G. van Sloun, R. Cohen, and Y. C. Eldar, "Deep learning in ultrasound imaging," *Proc. IEEE*, vol. 108, no. 1, pp. 11–29, 2020.
- [46] S. Gu, L. Zhang, W. Zuo, and X. Feng, "Weighted Nuclear norm minimization with application to image denoising," in *Proc. of the IEEE Conf. on Comput. Vision and Pattern Recognition*, 2014, pp. 2862–2869.
- [47] S. Wang, Y. Wang, Y. Chen, P. Pan, Z. Sun, and G. He, "Robust PCA using matrix factorization for background/foreground separation," *IEEE Access*, vol. 6, pp. 18 945–18 953, 2018.
- [48] D. Wipf and S. Nagarajan, "Iterative reweighted ℓ_1 and ℓ_2 methods for finding sparse solutions," *IEEE J. Sel. Topics Signal Process.*, vol. 4, no. 2, pp. 317–329, 2010.
- [49] M. Malek-Mohammadi, M. Babaie-Zadeh, and M. Skoglund, "Iterative concave rank approximation for recovering low-rank matrices," *IEEE Trans. on Signal Process.*, vol. 62, no. 20, pp. 5213–5226, 2014.
- [50] M. Fazel, H. Hindi, and S. P. Boyd, "Log-det heuristic for matrix rank minimization with applications to Hankel and Euclidean distance matrices," *Proc. of the 2003 American Control Conf.*, 2003., vol. 3, pp. 2156–2162 vol.3, 2003.
- [51] C. Lu, J. Tang, S. Yan, and Z. Lin, "Nonconvex nonsmooth low rank minimization via iteratively reweighted Nuclear norm," *IEEE Trans. Image Process.*, vol. 25, no. 2, p. 829–839, 2016. [Online]. Available: <http://dx.doi.org/10.1109/TIP.2015.2511584>
- [52] C. Lu, J. Tang, S. Yan, and Z. Lin, "Nonconvex nonsmooth low rank minimization via iteratively reweighted Nuclear norm," *IEEE Trans. on Image Process.*, vol. 25, no. 2, pp. 829–839, 2016.
- [53] Y. Sun, P. Babu, and D. P. Palomar, "Majorization-minimization algorithms in signal processing, communications, and machine learning," *IEEE Trans. on Signal Process.*, vol. 65, no. 3, pp. 794–816, 2017.
- [54] K. Chen, H. Dong, and K. Chan, "Reduced rank regression via adaptive Nuclear norm penalization," *Biometrika*, vol. 100, no. 4, pp. 901–920, 2013.
- [55] Y. Peng, J. Suo, Q. Dai, and W. Xu, "Reweighted low-rank matrix recovery and its application in image restoration," *IEEE Trans. on Cybernetics*, vol. 44, no. 12, pp. 2418–2430, 2014.
- [56] H. Wang, F. Zhang, Q. Wu, Y. Hu, and Y. Shi, "Nonconvex and nonsmooth sparse optimization via adaptively iterative reweighted methods," *arXiv preprint arXiv:1810.10167*, 2018.
- [57] D. P. Kingma and J. Ba, "Adam: A Method for Stochastic Optimization," *arXiv preprint arXiv:1412.6980*, 2017.
- [58] The MathWorks Inc, "Matlab: version 9.6.0 (r2019a)," 2019.
- [59] M. Grant and S. Boyd, "CVX: Matlab software for disciplined convex programming, version 2.1," Mar. 2014.
- [60] A. Paszke et al., "Pytorch: An imperative style, high-performance deep learning library," in *Advances in Neural Information Processing Systems 32*, H. Wallach, H. Larochelle, A. Beygelzimer, F. d'Alché-Buc, E. Fox, and R. Garnett, Eds. Curran Associates, Inc., 2019, pp. 8024–8035.
- [61] H. Robbins and S. Monro, "A stochastic approximation method," *The Annals of Mathematical Statistics*, pp. 400–407, 1951.
- [62] I. Sutskever, J. Martens, G. Dahl, and G. Hinton, "On the importance of initialization and momentum in deep learning," in *Int. Conf. on Machine Learning*. PMLR, 2013, pp. 1139–1147.